

Construction of High T_g Bipolar Host Materials with Balanced Electron–Hole Mobility Based on 1,2,4-Thiadiazole for Phosphorescent Organic Light-Emitting Diodes

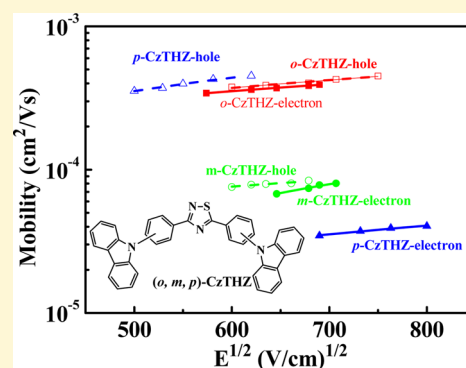
Jiangjiang Jin,[†] Wenzhi Zhang,[†] Bo Wang,[†] Guanyuan Mu,[†] Peng Xu,[†] Lei Wang,^{*,†} Hong Huang,[†] Jiangshan Chen,^{*,‡} and Dongge Ma[‡]

[†]Wuhan National Laboratory for Optoelectronics, School of Optical and Electronic Information, Huazhong University of Science and Technology, Wuhan, 430074 Hubei, P. R. China

[‡]State Key Laboratory of Polymer Physics and Chemistry, Changchun Institute of Applied Chemistry, Chinese Academy of Sciences, Changchun, 130022 Jilin, P. R. China

Supporting Information

ABSTRACT: A novel electron-transporting moiety, 1,2,4-thiadiazole, was first introduced to construct bipolar host molecules for phosphorescent organic light-emitting diodes (PhOLEDs). By incorporating 1,2,4-thiadiazole with typical hole-transporting carbazole moieties, a series of thiadiazole/carbazole hybrids, *o*-CzTHZ, *m*-CzTHZ, and *p*-CzTHZ, were synthesized. All the hybrids exhibit very high glass transition temperatures ($T_g \geq 167^\circ\text{C}$) and show good thermal and morphological stability in films. Moreover, these host materials possess good bipolar charge transporting properties; electron and hole mobilities of these bipolar thiadiazole/carbazole hybrids can be tuned by simply adjusting the linkage modes between thiadiazole and carbazole moieties. The maximum external quantum efficiencies ($\eta_{\text{EQE, max}}$) in the green PhOLEDs with *o*-CzTHZ, *m*-CzTHZ, and *p*-CzTHZ as the hosts reached 26.1%, 24.0%, and 22.9%, respectively, and their EQE were still over 20% even at the high luminance of 10,000 cd/m². This study demonstrates that 1,2,4-thiadiazole should be an excellent electron-transporting unit for bipolar phosphorescent hosts.



INTRODUCTION

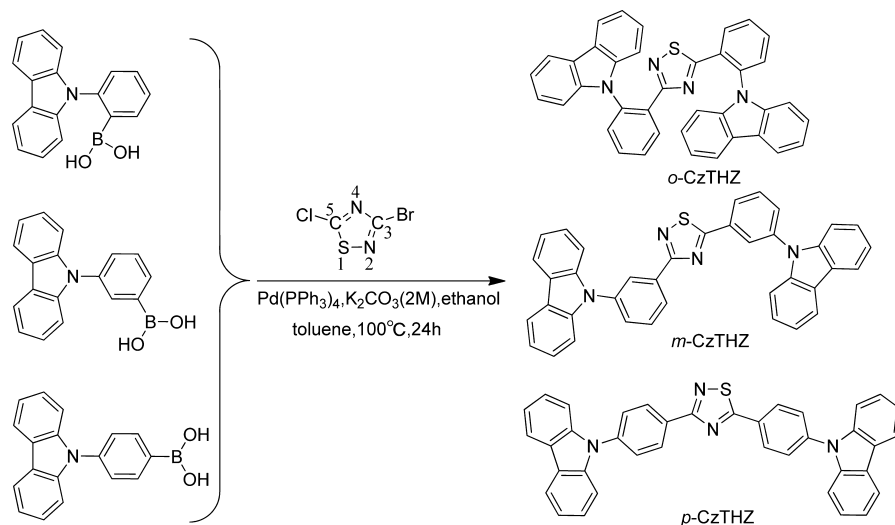
Phosphorescent organic light-emitting diodes (PhOLEDs) have continued to attract great interest because they can approach 100% internal quantum efficiency (IQE) by utilizing both singlet and triplet excitons.¹ To achieve highly efficient electrophosphorescence by reducing competitive factors, such as concentration quenching and triplet–triplet annihilation, phosphorescent emitters of heavy-metal complexes are usually doped into a suitable host material.² It is desirable that the host materials ought to have a large enough triplet energy gap for efficient energy transfer to the guest, good carrier transport properties for a balanced recombination of holes and electrons in the emitting layer, and energy-level matching with neighboring layers for effective charge injection.³ In recent years, the design of bipolar host materials configured with electron-donating groups as donors (D) and electron-withdrawing groups as acceptors (A) seems to be the most appealing strategy because they can provide more balance in electron and hole fluxes and simplify device structures.⁴ Electron-deficient moieties such as 1,3,4-oxadiazole,⁵ benzimidazole,⁶ pyridine,⁷ phenanthroimidazole,⁸ 1,3,5-triazine,⁹ and phosphine oxide¹⁰ have all been employed as efficient electron-transporting acceptors. Tao et al.^{5b} reported a carbazole/oxadiazole hybrid *o*-CzOXD for green PhOLEDs with Ir(ppy)₃

as the emitter, in which a maximum external quantum efficiency ($\eta_{\text{EQE, max}}$) of 20% and maximum power efficiency ($\eta_{\text{p, max}}$) of 59.3 lm/W were achieved. Additionally, they replaced the carbazole with triphenylamine to form another compound of *m*-TPA-*o*-OXD,¹¹ and the $\eta_{\text{EQE, max}}$ and $\eta_{\text{p, max}}$ were improved to 21% and 86.4 lm/W, respectively. Takizawa et al.¹² presented two green PhOLEDs based on the bipolar host materials, TPBI-Cz and TPBI-Da, showing maximum current efficiencies ($\eta_{\text{c, max}}$) of 48 cd/A and 60 cd/A, respectively. Chou et al.¹³ synthesized a bipolar material (BCPO) based on a carbazole/phosphine oxide hybrid, and the green PhOLED with BCPO as the host showed $\eta_{\text{EQE, max}}$ of 21.6%, $\eta_{\text{c, max}}$ of 83.4 cd/A and $\eta_{\text{p, max}}$ of 87.5 lm/W. In our previous work, a green device based on a bipolar host of mPhBINCP was reported,⁸ which exhibited a $\eta_{\text{c, max}}$ of 77.6 cd/A and a $\eta_{\text{EQE, max}}$ of 21%. The incorporation of hole-transporting and electron-transporting moieties into the multifunctional host materials has been proved to be an efficient method to broaden the recombination zone, improve the device efficiency, and simplify the device structure. Therefore, the development of bipolar

Received: October 24, 2013

Revised: March 14, 2014

Published: March 14, 2014

Scheme 1. Synthetic Routes to *o*-CzTHZ, *m*-CzTHZ, and *p*-CzTHZ

host materials containing new moieties is still interesting for practical applications. In addition, the thermal stability of the bipolar hosts ought to be further improved, which is advantageous to lengthen the lifetime of PhOLEDs for practical applications.

As we know, the carbazole group has been widely used in host materials because of its high triplet energy and excellent hole-transporting ability.¹⁴ For example, carbazole-based CBP has been used as the host for green and red phosphorescent emitters.¹⁵ However, the device performance with CBP was still unsatisfactory due to its low electron-transporting ability.¹⁶ Another disadvantage is the low glass transition temperatures (T_g) (about 62 °C) leading to easy crystallization, which is notorious for the poor lifetimes of PhOLEDs.¹⁷ Thus, the coupled electron-transporting groups should play very important roles to overcome the above issues in the carbazole-based bipolar hosts. Here, 1,2,4-thiadiazole as a novel electron-transporting group was first used to construct PhOLED bipolar host materials, and their optical and electronic performances have been studied systematically. We synthesized three carbazole/thiadiazole bipolar hosts, *o*-CzTHZ, *m*-CzTHZ, and *p*-CzTHZ, through adjusting the linkage mode between the carbazole and 1,2,4-thiadiazole moieties. Though these materials have relatively low molecular masses, their T_g values are as high as around 170 °C, which are much higher than those of the reported bipolar hosts. More interestingly, nearly equal hole and electron mobilities were realized in *o*-CzTHZ and *m*-CzTHZ, which will be expected to be beneficial for broadening recombination zones. Combining with the hole trapping-recombination, the $\eta_{\text{EQE, max}}$ in the green PhOLEDs with *o*-CzTHZ and *m*-CzTHZ as the bipolar hosts reached 26.1% and 24.0%, respectively, which could correspond to nearly 100% IQE. This study indicates that 1,2,4-thiadiazole is not only a novel electron-transporting moiety but also an excellent unit for building bipolar host materials with high thermal stability.

EXPERIMENTAL SECTION

General Procedures. ¹H NMR and ¹³C NMR spectra were conducted on a Bruker-AF301 AT 400 MHz spectrometer. Mass spectra were performed on an Agilent (1100 LC/MSD Trap) using APCI ionization. The experimental conditions and equipment used have been described in our previous works.^{8,14} Elemental analyses of

carbon, hydrogen, and nitrogen were measured on an Elementar (Vario Micro cube) analyzer. UV-vis absorption and PL spectra were recorded on a Shimadzu UV-vis-NIR spectrophotometer (UV-3600) and Edinburgh instruments (FLSP920 spectrometers), respectively. Cyclic voltammetry measurements were carried out on computer-controlled EG&G Potentiostat/Galvanostat model 283 at room temperature with a conventional three electrode cell consisting of a Pt button working electrode of 2 mm in diameter, a platinum wire counter electrode, and a Ag/AgNO₃ (0.1 M) reference electrode. Nitrogen-purged dichloromethane containing 0.1 M tetrabutylammoniumhexafluorophosphate (Bu₄NPF₆) was used as the supporting electrolyte. The redox potential was determined from the intersection of two tangents drawn at the rising and background current of the cyclic voltammogram. Differential scanning calorimetry (DSC) was recorded on a PE Instruments DSC 2920 unit with a heating rate of 10 °C/min from 25 to 250 °C under nitrogen. The glass transition temperature (T_g) was determined from the second heating scan. Thermogravimetric analysis (TGA) was undertaken using a PerkinElmer Instruments (Pyris1 TGA) at a heating rate of 10 °C/min from 30 to 700 °C under a nitrogen environment. The thermal stability of the samples were determined by the recorded temperature at 5% weight loss. In the time-of-flight (TOF) transient-photocurrent technique, those samples were illuminated at 355 nm through the ITO electrode from an UV-FQ q-switched DPSS laser (pulse: 4 ns). The transient currents were measured using a digital phosphor oscilloscope (DPO 3034; bandwidth: 300 MHz).

Synthesis. All the reagents and materials were received from Aldrich and used without further purification unless otherwise noted. 1,2,4-Thiadiazole was purchased from Wuhan Sunshine optoelectronics Technology Co. Ltd. Synthetic routes of the three compounds are outlined in Scheme 1.

2,5-Bis(2-(9H-carbazol-9-yl)phenyl)-1,2,4-thiadiazole (*o*-CzTHZ). A mixture of 3-bromo-5-chloro-1,2,4-thiadiazole (0.50 g, 2.5 mmol), (2-(9H-carbazol-9-yl)phenyl)boronic acid (1.61 g, 5.6 mmol), [Pd(PPh₃)₄] (196 mg, 0.17 mmol), K₂CO₃ (2.0 M aqueous solution, 5.0 mL, 10.0 mmol), toluene (50 mL), and ethanol (25.0 mL) was stirred at 100 °C for 24 h. After cooling to room temperature, dichloromethane (200.0 mL) was added to the reaction mixture. The organic phase was separated and washed with brine before being dried over anhydrous MgSO₄. The solvent was evaporated, and the solid residues were purified by column chromatography on silica gel with petroleum ether:dichloromethane (2:1) to afford the product as a white powder (1.28 g, 89%). ¹H NMR (400 MHz, DMSO-*d*⁶) δ [ppm]: 8.24–8.22 (d, *J* = 8.0 Hz, 2H), 8.19–8.15 (t, *J* = 6.4 Hz, 3H), 7.86–7.82 (t, *J* = 6.0 Hz, 1H), 7.77–7.69 (m, 3H), 7.49–7.45 (t, *J* = 6.4 Hz, 1H), 7.35–7.21 (m, 9H), 7.10–7.08 (d, *J* = 8.0 Hz, 1H), 6.92–6.90 (d, *J* = 8.0 Hz, 2H), 6.64–6.62 (d, *J* = 8.0 Hz, 2H); ¹³C NMR (100 MHz, CDCl₃) δ

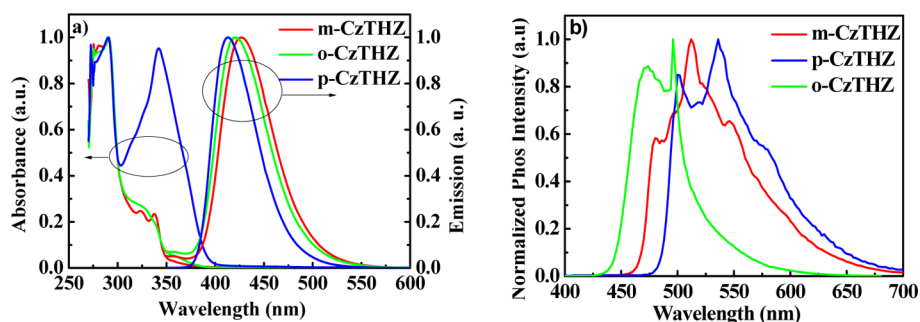


Figure 1. a) Absorption and emission spectra of *o*-CzTHZ, *m*-CzTHZ, and *p*-CzTHZ in toluene solution at room temperature. b) Phosphorescence spectra of *o*-CzTHZ, *m*-CzTHZ, and *p*-CzTHZ in 2-methyltetrahydrofuran at 77 K.

[ppm]: 180.97, 168.69, 142.17, 140.70, 136.08, 135.99, 132.05, 132.14, 131.70, 131.17, 130.47, 129.51, 129.41, 129.18, 128.72, 126.35, 125.78, 124.50, 123.35, 120.78, 120.42, 119.89, 110.00, 109.72; APCI MS (*m/z*): 569.5; Elemental analysis calcd (%) for $C_{38}H_{24}N_4S$: C 80.26, H 4.25, N 9.85; found: C 80.26, H 4.24, N 9.83.

2,5-Bis(3-(*H*-carbazol-9-yl)phenyl)-1,2,4-thiadiazole (*m*-CzTHZ). Compound *m*-CzTHZ was prepared according to the same procedure as compound *o*-CzTHZ but using (3-(9H-carbazol-9-yl)phenyl)boronic acid instead of (2-(9H-carbazol-9-yl)phenyl)boronic acid.

Yield: 84%; 1H NMR (400 MHz, $CDCl_3$) δ [ppm]: 8.60 (s, 1H), 8.48–8.46 (d, $J = 8.0$ Hz, 1H), 8.27 (s, 1H), 8.16–8.13 (d, $J = 8.0$ Hz, 4H), 8.11–8.09 (m, 1H), 7.75–7.74 (d, $J = 8.0$ Hz, 2H), 7.72–7.66 (m, 2H), 7.46–7.38 (m, 8H), 7.32–7.26 (m, 4H); ^{13}C NMR (100 MHz, $CDCl_3$) δ [ppm]: 187.43, 173.11, 140.91, 140.69, 139.01, 138.34, 134.61, 132.45, 130.99, 130.55, 130.31, 129.13, 127.38, 127.20, 126.43, 126.22, 126.05, 125.99, 123.65, 123.51, 120.48, 120.40, 120.33, 120.06, 109.78, 109.54; APCI MS (*m/z*): 569.2 [M+] $^+$; Elemental analysis calcd (%) for $C_{38}H_{24}N_4S$: C 80.26, H 4.25, N 9.85; found: C 80.27, H 4.26, N 9.85.

2,5-Bis(4-(*H*-carbazol-9-yl)phenyl)-1,2,4-thiadiazole (*p*-CzTHZ). Compound *p*-CzTHZ was prepared according to the same procedure as compound *o*-CzTHZ but using (4-(9H-carbazol-9-yl)phenyl)boronic acid instead of (2-(9H-carbazol-9-yl)phenyl)boronic acid.

Yield: 80%. 1H NMR (400 MHz, $CDCl_3$) δ [ppm]: 8.67–8.65 (d, $J = 8.0$ Hz, 2H), 8.33–8.31 (d, $J = 8.0$ Hz, 2H), 8.17–8.15 (d, $J = 8.0$ Hz, 4H), 7.80–7.74 (m, 4H), 7.53–7.51 (d, $J = 8.0$ Hz, 4H), 7.47–7.41 (m, 4H), 7.35–7.29 (m, 4H); ^{13}C NMR (100 MHz, $CDCl_3$) δ [ppm]: 187.38, 173.23, 141.25, 140.63, 140.36, 139.75, 131.69, 130.01, 129.26, 129.16, 127.47, 127.09, 126.26, 126.11, 123.89, 123.70, 120.65, 120.52, 120.40, 120.29, 109.86, 109.75; APCI MS (*m/z*): 569.7; Elemental analysis calcd (%) $C_{38}H_{24}N_4S$: C 80.26, H 4.25, N 9.85; found: C 80.25, H 4.26, N 9.84.

Quantum Calculation. Theoretical calculations on the geometrical and electronic properties were performed on the Amsterdam Density Functional (ADF) 2009.01 program package. B3LYP (Becke three parameters hybrid functional with Lee-Yang-Perdew correlation functionals) and the 6-31G(d) atomic basis set were used to determine and optimize the structures.¹⁸ Molecular orbitals were visualized using ADFView.

OLED Fabrication and Measurement. The EL devices were fabricated by vacuum thermal evaporation technology according to the methods modified from our previous approach.^{8,14} Devices with an area of 3 mm \times 3 mm were fabricated by vacuum deposition at 5×10^{-6} Torr. An indium tin oxide (ITO) with a sheet resistance of 20 Ω /square was used as the substrate. The ITO glass substrates were cleaned with acetone, ethanol, and deionized water and then dried in an oven at 120 $^\circ$ C. Before device fabrication, the clear ITO was treated with oxygen plasma for 5 min. The deposition rate of organic compounds was 0.9–1.1 Å s^{-1} . MnO_3 was deposited on the ITO surface and then followed by the other organic layers. Finally, a cathode composed of LiF and Al metal was deposited sequentially onto the substrate. The L–V–J of the devices was tested using a Keithley 2400 Source meter and PR655 under ambient conditions.

RESULTS AND DISCUSSION

Synthesis. The hybrids of *o*-CzTHZ, *m*-CzTHZ, and *p*-CzTHZ were synthesized by a Suzuki coupling reaction of 3-bromo-5-chloro-1,2,4-thiadiazole with carbazole intermediates, to give the desired compounds with excellent isolated yields. Carbazole intermediates were prepared according to a previously reported procedure.¹⁹ The detailed procedures and characterization of these new compounds are described in the Experimental Section. Repeated temperature-gradient vacuum sublimation is required for further purification of these materials used in PhOLEDs.

Photophysical and Electrochemical Properties. Figure 1 shows the electronic absorption and fluorescence spectra of the compounds *o*-CzTHZ, *m*-CzTHZ, and *p*-CzTHZ. The absorption at around 290 nm for all of the compounds could be assigned to the carbazole-centered $n-\pi$ transition. The longer-wavelength absorption at around 330–340 nm could be attributed to the $\pi-\pi^*$ transition from the electron-donating carbazole moiety to the electron-accepting thiadiazole moiety. The assignment is manifested by the fact that the intensity of the $\pi-\pi^*$ transition for *o*-CzTHZ and *m*-CzTHZ is remarkably reduced in comparison to the dominant $\pi-\pi^*$ transition for *p*-CzTHZ. This may be ascribed to the good π -conjugation between the carbazole and thiadiazole moieties when the carbazole is linked at the *para* position of the 3,5-diphenyl-1,2,4-thiadiazole for *p*-CzTHZ.

All of the compounds emit deep-blue light with the emission peaks in the range of 410–430 nm in the solution state. The triplet energies (E_T), determined by the highest-energy vibronic sub-band of the phosphorescence spectra at 77 K, follow the trend: *o*-CzTHZ (2.62 eV) > *m*-CzTHZ (2.58 eV) > *p*-CzTHZ (2.48 eV), implying that they may act as appropriate host materials for green and red phosphorescent emitters. The E_T of *o*-CzTHZ is higher than those of *m*-CzTHZ and *p*-CzTHZ, which is most likely due to the strong steric effects in *o*-CzTHZ.²⁰

Electrochemical Properties. Cyclic voltammetry (CV) was performed to study the electrochemical properties of bipolar host materials *o*-CzTHZ, *m*-CzTHZ, and *p*-CzTHZ. Their cyclic voltammograms are shown in Figure 2, and the respective electrochemical data are summarized in Table 1. All compounds exhibited irreversible oxidation peaks at around 1.0 V, which is most likely resulting from the electrochemical property of the carbazole moiety.²¹ The irreversible oxidations of the three bipolar molecules were due to the dimerization or electropolymerization of the carbazole units at the C3 and/or C6 positions.^{6a} On the other hand, both *o*-CzTHZ, *m*-CzTHZ, and *p*-CzTHZ exhibited a well-defined quasireversible reduc-

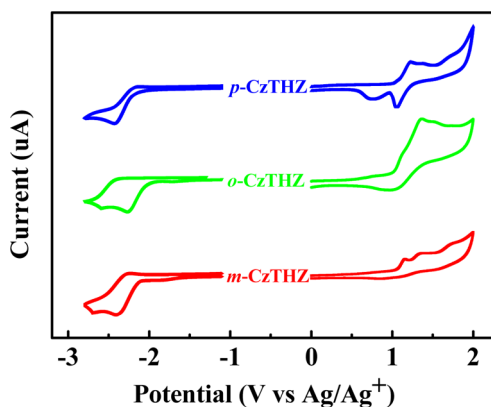


Figure 2. Cyclic voltammograms of *o*-CzTHZ, *m*-CzTHZ, and *p*-CzTHZ in CH_2Cl_2 solution.

tion process at -2.04 , -2.18 , and -2.13 V (vs Ag/AgNO_3), respectively, which is dependent on the linkage modes of the carbazole and 1,2,4-thiadiazole. The highest occupied molecular orbital (HOMO) and the lowest unoccupied molecular orbital (LUMO) energy levels of these compounds were calculated from the onset potentials of oxidation and reduction. The HOMO/LUMO levels were estimated to be $-5.64/-2.64$, $-5.51/-2.50$, and $-5.50/-2.55$ eV, respectively, by comparing with ferrocene (Fc) (HOMO = $-(E_{\text{ox}} + 4.68)$ eV) and ferrocene (Fc) (LUMO = $-(E_{\text{red}} + 4.68)$ eV). This implies that holes and electrons can transfer into the bipolar hosts with small obstruction from TCTA ($-5.3/-2.36$ eV) and TmPyPB ($-6.68/-2.73$ eV),²² respectively, and then be well-confined in the emissive layers.

Theoretical Calculations. To gain insight into the electronic structures of these compounds, a density functional theory (DFT) calculation was performed. As shown in Figure 3, the calculated HOMO/LUMO values are in the range of $5.38-5.55/2.55-2.64$ eV, which also correlates well with the experimental data. The electron distributions in the HOMO level for these new compounds are located on the phenyl-carbazole linked to the C3 of 1,2,4-thiadiazole, and in the LUMO the electron distributions are mostly located on 1,2,4-thiadiazole and phenyl linked to C5 of 1,2,4-thiadiazole, which could be ascribed to the more strong electronegativity of the C3 of 1,2,4-thiadiazole. All of these materials have almost complete separation of the HOMO and LUMO. The separation between the HOMO and LUMO is beneficial for efficient charge-carrier transport and the prevention of reverse energy transfer.²³

Thermal Properties. The thermal properties of *o*-CzTHZ, *m*-CzTHZ, and *p*-CzTHZ were determined by thermogravimetric analysis (TGA) and differential scanning calorimetry (DSC), as shown in Figure 4. The decomposition temperatures (T_d , corresponding to 5% weight loss) and the T_g are also listed in Table 1. The T_d of *o*-CzTHZ, *m*-CzTHZ, and *p*-CzTHZ are

in the range of $370-420$ °C, and their corresponding T_g are 167, 170, and 168 °C, respectively. The T_g values of these new compounds are much higher than those of the most reported bipolar hosts, such as the analogous oxadiazole/cabazole hybrids (*o*-CzOXD, *p*-CzOXD and *m*-CzOXD).^{5b} This clearly indicates that the 1,2,4-thiadiazole moiety should play a dominant role in the thermal properties of the bipolar host materials. The high T_d and T_g highlight the suitability of these materials to render high quality amorphous thin films upon vacuum thermal evaporation, which is the prerequisite for the preparation of devices with high efficiency and high stability.

To get an insight into the thermal stabilities of the vacuum evaporated films of *o*-CzTHZ, *m*-CzTHZ, and *p*-CzTHZ, the effects of annealing temperatures on the morphologies were studied by atomic force microscopy (AFM). As shown in Figure 5, the pristine solid films of *o*-CzTHZ, *m*-CzTHZ, and *p*-CzTHZ exhibit a fairly smooth surface morphology with the root-mean-square (RMS) roughness of 0.429, 0.469, and 0.415 nm, respectively. After thermal annealing at 150 °C for 30 min under a nitrogen atmosphere, the RMS roughness of the corresponding films are still as low as 0.638, 0.449, and 0.641 nm, respectively. These results indicate that all three hosts have excellent thermal and morphological stability, which would be advantageous to the stability of PhOLEDs.

Bipolar Transporting Characteristics. In order to study the bipolar transporting properties of *o*-CzTHZ, *m*-CzTHZ, and *p*-CzTHZ, the time-of-flight (TOF) technique was used to determine their charge carrier mobilities. Figure 6 shows typical TOF transients of hole/electron for *o*-CzTHZ, *m*-CzTHZ, and *p*-CzTHZ under an applied field. Figure 7 shows the hole and electron mobilities of *o*-CzTHZ, *m*-CzTHZ, and *p*-CzTHZ plotted as a function of the square root of the applied electric field.

The almost balanced hole and electron mobilities were found for *o*-CzTHZ. The hole mobilities of *o*-CzTHZ are in the range of 3.72×10^{-4} to 4.47×10^{-4} $\text{cm}^2/(\text{V s})$ with fields varying from 3.6×10^5 to 5.6×10^5 V/cm, and the electron mobilities are in the range of 3.41×10^{-4} to 3.91×10^{-4} $\text{cm}^2/(\text{V s})$ with fields varying from 3.3×10^5 to 4.7×10^5 V/cm. The values of hole and electron mobilities for *m*-CzTHZ are also very close, in which its hole mobilities lie in the range of 7.61×10^{-5} to 8.31×10^{-5} $\text{cm}^2/(\text{V s})$ during $3.6-4.6 \times 10^5$ V/cm, and its electron mobilities lie in the range of 6.78×10^{-5} to 8.06×10^{-5} $\text{cm}^2/(\text{V s})$ during $4.2-5.0 \times 10^5$ V/cm. These results indicate that the *o*-CzTHZ and *m*-CzTHZ show bipolar charge-transport properties with excellent balanced electron and hole mobilities. The hole mobilities of *p*-CzTHZ lie in the range of 3.52×10^{-4} to 4.56×10^{-4} $\text{cm}^2/(\text{V s})$ when the fields vary from 2.5×10^5 to 3.8×10^5 V/cm, while the electron mobilities lie in the range of 2.46×10^{-5} to 3.28×10^{-5} $\text{cm}^2/(\text{V s})$ with fields varying from 4.8×10^5 to 6.4×10^5 V/cm, which means that the hole mobilities are an order of magnitude higher than the electron mobilities. This study demonstrates that the

Table 1. Photophysical, Electrochemical, and Thermal Properties of the *o*-CzTHZ, *m*-CzTHZ, and *p*-CzTHZ

	Abs ^a (nm)	PL ^a (nm)	E_{ox}^b (V)	E_{red}^b (V)	HOMO/LUMO (eV)	HOMO/LUMOCAL ^c (eV)	E_g^d (eV)	E_T^e (eV)	T_d/T_g^f (°C)
<i>o</i> -CzTHZ	330/291	421	0.96	-2.04	-5.64/-2.64	-5.55/-2.84	3.00	2.62	370/167
<i>m</i> -CzTHZ	338/281	428	0.83	-2.18	-5.51/-2.50	-5.38/-2.58	3.01	2.58	394/170
<i>p</i> -CzTHZ	342/290	413	0.82	-2.13	-5.50/-2.55	-5.43/-2.67	2.95	2.48	420/168

^aMeasured in CH_2Cl_2 . ^bThe onset potential of oxidation and reduction as referenced to ferrocene (Fc). ^cValues from DFT calculation. ^dThe band gap energies were estimated from CV. ^eMeasured in 2-MeTHF at 77 K. ^fMeasured from DSC and TGA.

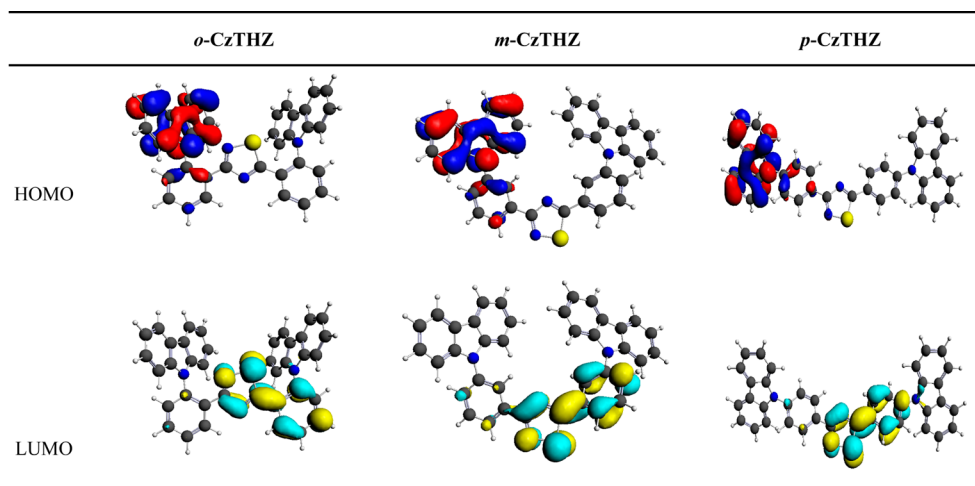


Figure 3. Spatial distributions of the HOMO and LUMO levels for *o*-CzTHZ, *m*-CzTHZ, and *p*-CzTHZ.

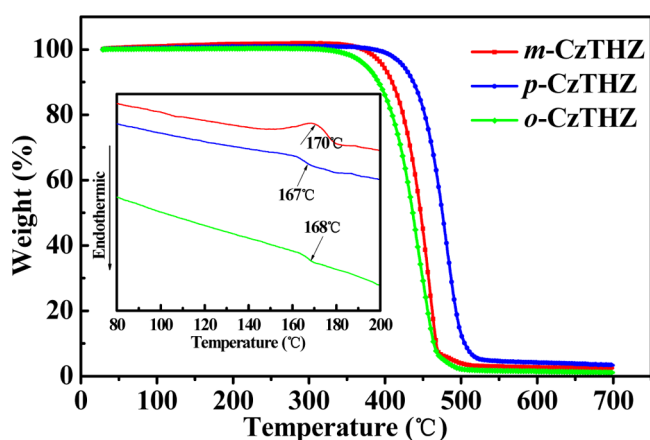


Figure 4. TGA thermograms of *o*-CzTHZ, *m*-CzTHZ, and *p*-CzTHZ recorded at a heating rate of $10\text{ }^{\circ}\text{C min}^{-1}$. Inset: DSC thermograms of *o*-CzTHZ, *m*-CzTHZ, and *p*-CzTHZ recorded at a heating rate of $10\text{ }^{\circ}\text{C min}^{-1}$.

bipolar charge transporting properties of the thiazole/carbazole hybrids can be simply adjusted by the linkage mode. The relatively high carrier mobility of *o*-CzTHZ will be beneficial for the fabrication of a high efficiency device.

Electrophosphorescent OLED Characterization. To evaluate the performance of the thiazole/carbazole asymmetric hybrids as hosts, PhOLEDs were fabricated by using a green emitter of $\text{Ir}(\text{ppy})_3$ as the guest. The device configuration is ITO/ MoO_3 (10 nm)/TAPC (50 nm)/TCTA (5 nm)/Host: $x\text{ Ir}(\text{ppy})_3$ (20 nm)/TmPyPB (45 nm)/LiF (1 nm)/Al (100 nm) (*o*-CzTHZ for device A, *m*-CzTHZ for device B, and *p*-CzTHZ for device C). The energy level diagram is shown in Figure 8. TAPC (4,4'-cyclohexylidenebis[N,N-bis(4-methylphenyl)benzenamine]) was used as the hole-transporting material, TmPyPB (1,3,5-tri[(3-pyridyl)phen-3-yl]-benzene) was used as both the electron-transporting and hole-blocking layer, and MoO_3 and LiF served as the hole and electron-injecting layers, respectively. In the devices, TCTA (tris(4-carbazoyl-9-ylphenyl)amine) was chosen as the exciton blocker to prevent the diffusion of excitons to the hole-

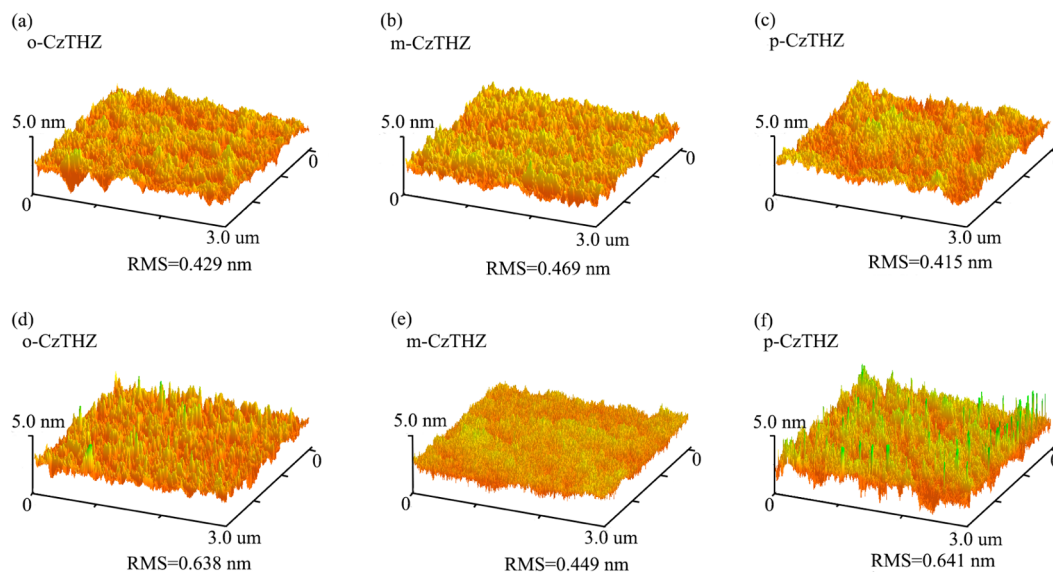


Figure 5. Atomic force microscopic pictures of *o*-CzTHZ, *m*-CzTHZ, and *p*-CzTHZ. (a), (b), (c) without thermal treatment and (d), (e), (f) after thermal treatment at $150\text{ }^{\circ}\text{C}$ for 30 min.

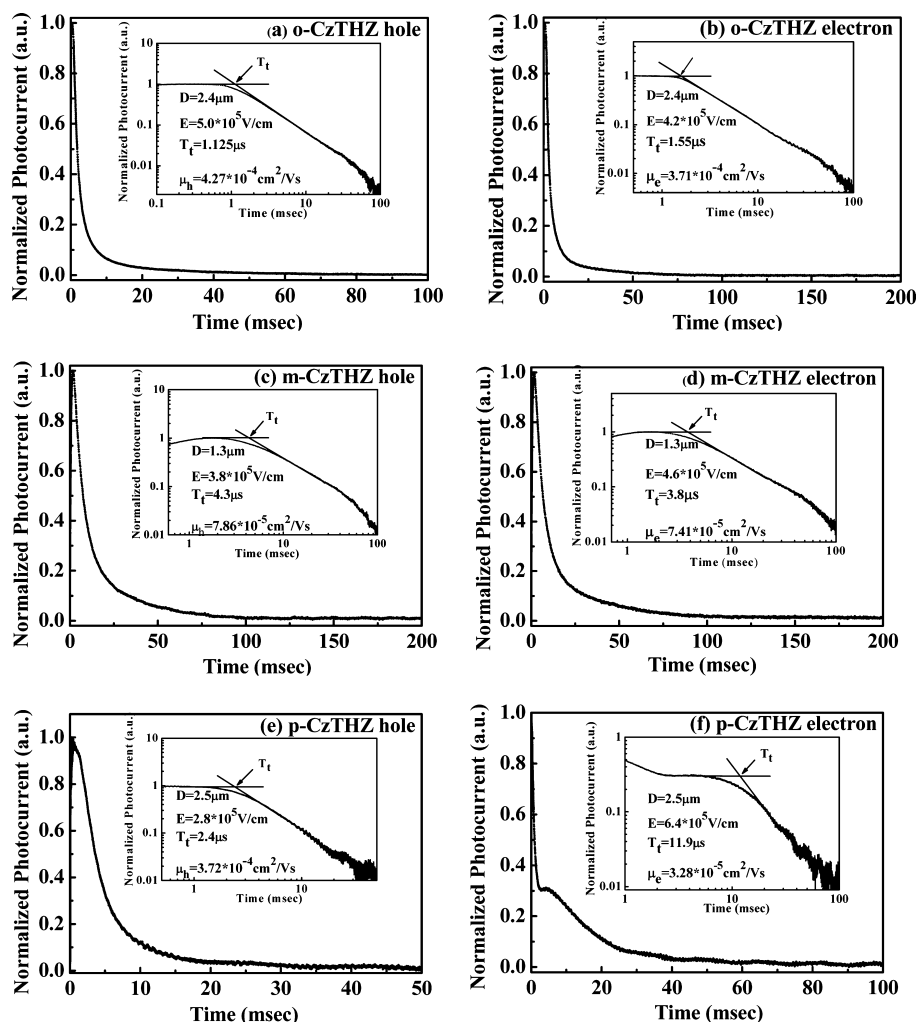


Figure 6. Log of the photocurrent vs the log of time in a time-of-flight measurement. The electron mobility (μ) was calculated from the values of the transit time (T_t), the sample thickness, and the applied voltage (V) according to the equation $\mu = D^2/(VT_t)$.

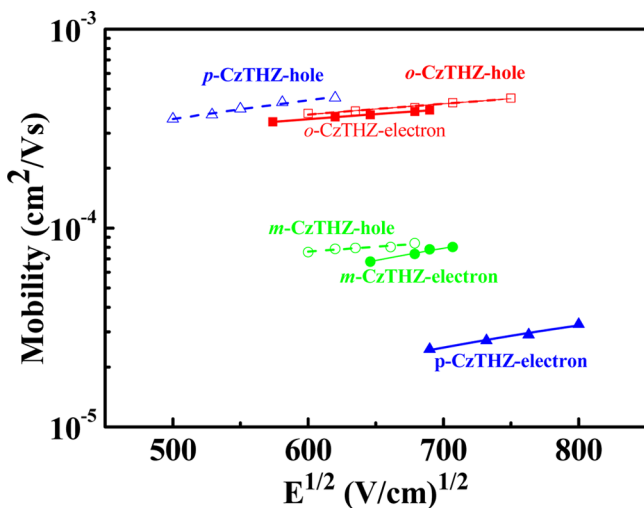


Figure 7. Electron and hole mobilities versus $E^{1/2}$ for o-CzTHZ, m-CzTHZ, and p-CzTHZ.

transporting layer. Meanwhile, TCTA can also reduce the hole injection barrier from TAPC to the host. The dopant concentration was optimized through concentration-dependent experiments with the dopant amount ranging from 3 to 9 wt %.

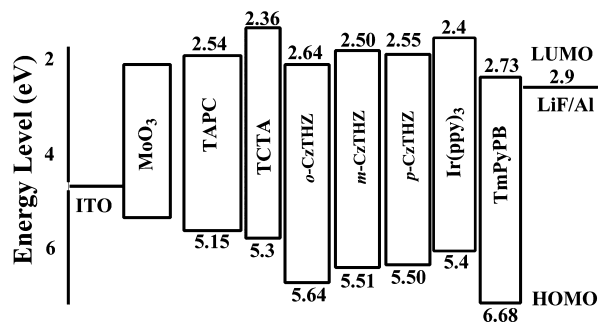


Figure 8. Energy level diagram of the devices based on the 1,2,4-thiadiazole derivatives.

The 3 wt %-doped device (A_1-C_1) shows good efficiencies, and the EQE of the three hosts are all over 20%, but they are still lower than the 6 wt %-doped devices (A_2-C_2). This demonstrates that the triplet energy transfer from the host to the dopant is not complete. The 9 wt %-doped device (A_3-C_3) shows the lowest efficiencies, which suggests considerable self-quenching of the dopant upon excitation when excess Ir(ppy)₃ has been codeposited. Above all, we find that all the devices with 6 wt % dopant exhibit the best efficiencies (see Figure S3 and Table S1).

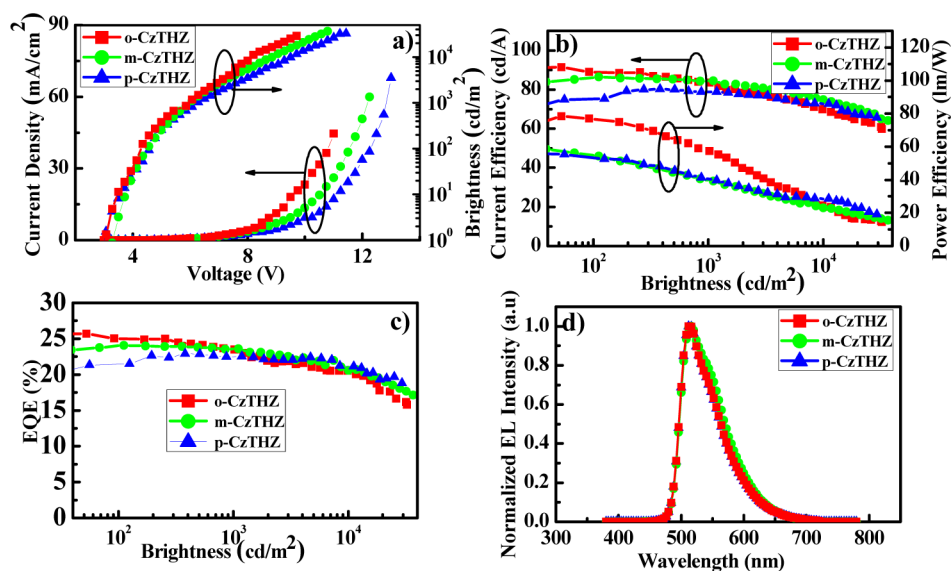


Figure 9. Green electrophosphorescence properties of devices A_2 , B_2 , and C_2 with *o*-CzTHZ, *m*-CzTHZ, and *p*-CzTHZ as the host: a) J–V–L curves; b) current efficiency and power efficiency versus brightness curves; c) EQE versus brightness curves; d) EL spectra.

Table 2. Electroluminescence Properties of the Devices A_2 – C_2 ^a

device	host	V_{on} [V]	$[\eta_c]^b$ [cd/A]	$[\eta_p]^b$ [lm/W]	$[\eta_{EQE}]^b$ [%]	$[\eta_{EQE}]^c$ [%]	CIE [x, y] ^d
A_2	<i>o</i> -CzTHZ	3.1	92.3(±1.2%)	78.8(±0.4%)	26.1(±1.5%)	20.3(±0.5%)	(0.30, 0.62)
B_2	<i>m</i> -CzTHZ	3.4	86.4(±1.3%)	61.8(±1.4%)	24.0(±0.8%)	20.6 (±0.5%)	(0.31, 0.62)
C_2	<i>p</i> -CzTHZ	3.1	80.2(±0.2%)	56.7(±0.3%)	22.9(±0.9%)	21.2 (±0.5%)	(0.30, 0.62)

^a V_{on} : turn-on voltage at 1 cd/m²; η_c : current efficiency; η_p : power efficiency. ^bOrder of measured value: maximum. ^cMeasured at 10000 cd/m². ^dMeasured at 100 cd/m².

As shown in Figure 9 and Table 2, the optimized devices A_2 – C_2 display turn-on voltages from 3.1–3.4 V, and the efficiencies of them are in the order: $A_2 > B_2 > C_2$. Device A_2 based on *o*-CzTHZ achieves a $\eta_{c, max}$ of 92.3 cd/A and a $\eta_{p, max}$ of 78.8 lm/W, particularly, its $\eta_{EQE, max}$ reaches 26.1%. The maximum efficiencies for devices B_2 and C_2 are 86.4 cd/A (61.8 lm/W and 24.0%) and 80.2 cd/A (56.7 lm/W and 22.9%), respectively. Even at a high brightness of 10000 cd/m², the EQE of devices A_2 , B_2 , and C_2 are still as high as 20.3%, 20.6%, and 21.2%, respectively, indicating the devices show low efficiency roll-off.

The reason why the *o*-CzTHZ based device possesses the best efficiencies can be elucidated from the following aspects. First, the higher triplet energies of *o*-CzTHZ could efficiently suppress adverse energy back-transfer from the guest Ir(pp_y)₃ (2.40 eV)²⁴ to the host, consequently resulting in good performances of device A_2 . Second, the host *o*-CzTHZ exhibits higher charge mobilities than that of *m*-CzTHZ and *p*-CzTHZ, as shown in Figure 7. Third, the hole trapping-recombination mechanism for *o*-CzTHZ is another factor that affects the efficiency of device A_2 . To confirm the hypothesis, the hole-only device of ITO/MoO₃ (5 nm)/TCTA (10 nm)/Hosts: Ir(pp_y)₃ (0%, 6%) (40 nm)/TCTA (10 nm)/MoO₃ (5 nm)/Al was fabricated. As depicted in Figure S5, it can be clearly seen that the current density of a doped hole-only device based on *o*-CzTHZ reduces more obviously than that of *m*-CzTHZ and *p*-CzTHZ, which is induced by the deepest hole traps of *o*-CzTHZ. At the low current density, hole-trapping could provide an additional emission process and will improve the efficiency.²⁵ Regrettably, the more trapped holes will lead to triplet-charge annihilation and induce the efficiency roll-off

when the current density increased. It should be noted that the hole mobility of TAPC²⁶ is higher than the electron mobility of TmPyPb;²⁷ therefore, the more stronger hole trap of *o*-CzTHZ may be beneficial to the hole/electron balance in the emissive layer.

Peak wavelengths of the EL spectra of green devices A_2 – C_2 exhibit an emission similar to the phosphorescent emitter Ir(pp_y)₃. This suggests that the emission peaks are indeed derived from the dopant, and the triplet energy transfer from the hosts to the dopant are complete. The current density–voltage–luminance (J–V–L) characteristics, efficiency–luminance characteristics, and EL spectra of the devices are shown in Figure 9, and the key parameters are summarized in Table 2. In order to reflect the reproducibility of the higher efficiencies based on 6 wt %–doped Ir(pp_y)₃, all three hosts were tested for three times under the same conditions, which can be seen from Figure 9, Figure S4, and Table S2, and the efficiencies all exhibit only small deviations.

CONCLUSIONS

In conclusion, the 1,2,4-thiadiazole moiety was employed as the electron-transporting moiety for bipolar host materials, and a series of simple thiadiazole/carbazole hybrids were developed. Their bipolar charge transporting properties can be tuned by changing the linkage mode and the balanced electron, and hole mobilities were achieved when carbazole was attached to 1,2,4-thiadiazole *via ortho* and *para* positions. Besides, the introduction of the 1,2,4-thiadiazole moiety can significantly improve the thermal stability of the bipolar host materials, which is beneficial to the device stability. The devices with *o*-CzTHZ, *m*-CzTHZ, and *p*-CzTHZ as the hosts achieve

$\eta_{\text{EQE, max}}$ as high as 26.1%, 24.0%, and 22.9%, respectively. In addition, these devices show reduced efficiency roll-off at high luminance. Our study reveals that 1,2,4-thiadiazole is an excellent electron-transporting moiety for constructing bipolar host materials with high thermal stability and balanced charge transporting properties and suggests that 1,2,4-thiadiazole based materials could have great potential for use in PhOLEDs as phosphorescent hosts.

■ ASSOCIATED CONTENT

📄 Supporting Information

The HOMO and LUMO of TAPC and TCTA were measured cyclic voltammetry (CV) in CH_2Cl_2 , and their cyclic voltammograms are shown in Figures S1 and S2. PE-CE-Brightness, EQE-Brightness plots, and table of efficiencies. This material is available free of charge via the Internet at <http://pubs.acs.org>.

■ AUTHOR INFORMATION

Corresponding Authors

*E-mail: wanglei@mail.hust.edu.cn.

*E-mail: jschen@ciac.ac.cn.

Notes

The authors declare no competing financial interest.

■ ACKNOWLEDGMENTS

This research work was supported by the NSFC/China (21161160442, 51203056), the National Basic Research Program of China (973 Program 2013CB922104), and the Analytical and Testing Centre at Huazhong University of Science and Technology. The authors thank Dr. M. P. Aldred for the English polishing.

■ REFERENCES

- (1) (a) Su, Y. J.; Huang, H. L.; Li, C. L.; Chien, C. H.; Tao, Y. T.; Chou, P. T.; Datta, S.; Liu, R. S. *Adv. Mater.* **2003**, *15*, 884. (b) Yang, C. L.; Zhang, X. W.; You, H.; Zhu, L. Y.; Chen, L. Q.; Zhu, L. N.; Tao, Y. T.; Ma, D. G.; Shuai, Z. G.; Qin, J. G. *Adv. Funct. Mater.* **2007**, *17*, 651. (c) Zhou, G.; Wong, W. Y.; Yao, B.; Xie, Z.; Wang, L. *Angew. Chem., Int. Ed.* **2007**, *46*, 1149. (d) Baldo, M. A.; Lamansky, S.; Burrows, P. E.; Thompson, M. E.; Forrest, S. R. *Appl. Phys. Lett.* **1999**, *75*, 4. (e) Adachi, C.; Baldo, M. A.; Thompson, M. E.; Forrest, S. R. *J. Appl. Phys.* **2001**, *90*, 5048.
- (2) Su, S.-J.; Sasabe, H.; Takeda, T.; Kido, J. *Chem. Mater.* **2008**, *20*, 1691.
- (3) Chaskar, A.; Chen, H. F.; Wong, K. T. *Adv. Mater.* **2011**, *23*, 3876.
- (4) Lai, M. Y.; Chen, C. H.; Huang, W. S.; Lin, J. T.; Ke, T. H.; Chen, L. Y.; Tsai, M. H.; Wu, C. C. *Angew. Chem., Int. Ed.* **2008**, *47*, 581.
- (5) (a) Cheng, S.-H.; Chou, S.-H.; Hung, W.-Y.; You, H.-W.; Chen, Y.-M.; Chaskar, A.; Liu, Y.-H.; Wong, K.-T. *Org. Electron.* **2013**, *14*, 1086. (b) Tao, Y.; Wang, Q.; Yang, C.; Zhong, C.; Zhang, K.; Qin, J.; Ma, D. *Adv. Funct. Mater.* **2010**, *20*, 304.
- (6) (a) Chen, Y.-M.; Hung, W.-Y.; You, H.-W.; Chaskar, A.; Ting, H.-C.; Chen, H.-F.; Wong, K.-T.; Liu, Y.-H. *J. Mater. Chem.* **2011**, *21*, 14971. (b) Ge, Z.; Hayakawa, T.; Ando, S.; Ueda, M.; Akiike, T.; Miyamoto, H.; Kajita, T.; Kakimoto, M.-a. *Chem. Mater.* **2008**, *20*, 2532.
- (7) (a) Koech, P. K.; Polikarpov, E.; Rainbolt, J. E.; Cosimbescu, L.; Swensen, J. S.; Von Ruden, A. L.; Padmaperuma, A. B. *Org. Lett.* **2010**, *12*, 5534. (b) Park, M. S.; Lee, J. Y. *Org. Electron.* **2013**, *14*, 1291.
- (8) Huang, H.; Wang, Y.; Zhuang, S.; Yang, X.; Wang, L.; Yang, C. *J. Phys. Chem. C* **2012**, *116*, 19458.
- (9) Rothmann, M. M.; Haneder, S.; Da Como, E.; Lennartz, C.; Schildknecht, C.; Strohhriegel, P. *Chem. Mater.* **2010**, *22*, 2403.
- (10) (a) Jeong, S. H.; Lee, J. Y. *J. Mater. Chem.* **2011**, *21*, 14604. (b) Han, C.; Zhang, Z.; Xu, H.; Li, J.; Xie, G.; Chen, R.; Zhao, Y.; Huang, W. *Angew. Chem., Int. Ed.* **2012**, *51*, 10104.
- (11) Tao, Y.; Wang, Q.; Yang, C.; Zhong, C.; Qin, J.; Ma, D. *Adv. Funct. Mater.* **2010**, *20*, 2923.
- (12) Takizawa, S.-y.; Montes, V. A.; Anzenbacher, P. *Chem. Mater.* **2009**, *21*, 2452.
- (13) Chou, H. H.; Cheng, C. H. *Adv. Mater.* **2010**, *22*, 2468.
- (14) Huang, H.; Wang, Y. X.; Pan, B.; Yang, X.; Wang, L.; Chen, J. S.; Ma, D. G.; Yang, C. L. *Chem.—Eur. J.* **2013**, *19*, 1828.
- (15) Chou, H.-H.; Shih, H.-H.; Cheng, C.-H. *J. Mater. Chem.* **2010**, *20*, 798.
- (16) Kim, Y.-K.; Moon, B.-S.; Ha, C.-S. *J. Appl. Phys.* **2006**, *100*, 064511.
- (17) Zhou, G.; Wong, W.-Y.; Yao, B.; Xie, Z.; Wang, L. *Angew. Chem., Int. Ed.* **2007**, *46*, 1149.
- (18) (a) Lee, C.; Yang, W.; Parr, R. G. *Phys. Rev. B* **1988**, *37*, 785. (b) Soler, J. M.; Serena, P. A.; Garcia, N. *Phys. Rev. B* **1988**, *37*, 8701. (c) Boese, A. D.; Handy, N. C. *J. Chem. Phys.* **2002**, *116*, 9559. (d) Yang, X.; Huang, H.; Pan, B.; Zhuang, S. Q.; Wang, L.; Chen, J. S.; Ma, D. G. *J. Phys. Chem. C* **2012**, *116*, 15041.
- (19) You, J.; Li, G.; Wang, Z. *Org. Biomol. Chem.* **2012**, *10*, 9481.
- (20) Fan, C.; Zhao, F.; Gan, P.; Yang, S.; Liu, T.; Zhong, C.; Ma, D.; Qin, J.; Yang, C. *Chem.—Eur. J.* **2012**, *18*, 5510.
- (21) Mondal, E.; Hung, W.-Y.; Dai, H.-C.; Wong, K.-T. *Adv. Funct. Mater.* **2013**, *23*, 3096.
- (22) Bin, J. K.; Cho, N. S.; Hong, J. I. *Adv. Mater.* **2012**, *24*, 2911.
- (23) Ge, Z.; Hayakawa, T.; Ando, S.; Ueda, M.; Akiike, T.; Miyamoto, H.; Kajita, T.; Kakimoto, M.-a. *Adv. Funct. Mater.* **2008**, *18*, 584.
- (24) He, G.; Pfeiffer, M.; Leo, K.; Hofmann, M.; Birstock, J.; Pudzich, R.; Salbeck, J. *Appl. Phys. Lett.* **2004**, *85*, 3911.
- (25) (a) Han, C.; Zhao, F.; Zhang, Z.; Zhu, L.; Xu, H.; Li, J.; Ma, D.; Yan, P. *Chem. Mater.* **2013**, *25*, 4966. (b) Zhao, F.; Sun, N.; Zhang, H.; Chen, J.; Ma, D. *J. Appl. Phys.* **2012**, *112*, 084504. (c) Wang, Q.; Ding, J.; Ma, D.; Cheng, Y.; Wang, L.; Jing, X.; Wang, F. *Adv. Funct. Mater.* **2009**, *19*, 84.
- (26) Suh, M. C.; Shin, H. Y.; Cha, S. J. *Org. Electron.* **2013**, *14*, 2198.
- (27) Su, S.-J.; Chiba, T.; Takeda, T.; Kido, J. *Adv. Mater.* **2008**, *20*, 2125.